Preprint, accepted for publication in Shock Waves, March 2023.
Published version available online at
https://doi.org/10.1007/s00193-023-01126-5

Analysis of Shock Wave Acceleration from Normal Detonation Reflection

Donner T. Schoeffler[1*] and Joseph E. Shepherd[1]

[1*]California Institute of Technology, Pasadena, CA.

*Corresponding author(s). E-mail(s): dschoeff@caltech.edu;
Contributing authors: joseph.e.shepherd@caltech.edu;

Abstract

Normal detonation reflection generates a shock wave that exhibits complicated dynamics as it propagates through the incident detonation and post-detonation flow. Ideal models have historically neglected the influence of a finite detonation thickness on the reflected shock due to its small size relative to laboratory scales. However, one-dimensional numerical simulations show that the reflected shock accelerates to a large shock speed not predicted by ideal theory as it propagates through the incident detonation. Analysis with a derived shock-change equation identifies the principal role of the highly nonuniform upstream flow on producing the large shock acceleration. Simulations of detonation reflection show how a finite detonation thickness affects the entire trajectory of the reflected shock.

Keywords: Detonation reflection, Shock acceleration, Shock-change equations, Heterogeneous fluids

1 Introduction

The propagation of gaseous detonation waves down pipes is a common feature of laboratory detonation physics experiments and possible industrial accident scenarios. In nearly all cases, the detonation reaches the end of a pipe and impacts a high-impedance wall, where it reflects a shock wave that propagates backwards through the incident detonation and post-detonation flow. Normal detonation reflection is a fundamental example of both detonation-structure interactions and shock propagation through heterogeneous media. Despite the elementary nature of the problem and its ubiquitous occurrence in most detonation tube experiments, prior research has been sparse, and basic questions relating to the reflected shock's evolution remain unanswered.

Nearly all analytical modeling of the problem has focused on an idealization that the detonation itself is small relative to the length of the pipe, and so the reflected shock wave can be treated as if it originated immediately from reflection of the equilibrium, Chapman-Jouguet (CJ) state. From this formulation several solutions have been obtained since it considers shock reflection directly into the known Taylor-Zel'dovich (TZ) wave. Despite this, all models are inexact and make assumptions about the post-reflected-shock flow. Stanyukovich [1] first solved the problem by using the acoustic approximation for the reflected shock and assuming that the post-shock thermodynamic state was uniform. Shepherd et al. [2] performed numerical simulations of the fully nonlinear equations and also observed uniformity in the post-reflected-shock thermodynamic state, corroborating Stanyukovich's assumption. This observation was used by Karnesky et al. [3] to develop a quasi-empirical approach, where a pressure trace from the detonation-reflecting pipe end wall was utilized with

the assumption that the post-reflected-shock pressure was uniform. Strachan et al. [4] formulated a theory for shock propagation through a generally heterogeneous upstream flow by extending methods developed by Chisnell [5], which neglect influences behind the shock. Strachan et al. evaluated their theory using the idealized problem of detonation reflection and compared their model to experimental results. Schoeffler and Shepherd [6] instead assumed that the post-reflected-shock velocity gradient was uniform, which enabled a more generally applicable model using integration of an otherwise-exact shock-change equation. All of these models produce similar results since they use identical assumptions for the upstream flow and reflection from the CJ state.

Experiments have mostly been performed to investigate the structural dynamic loading induced by detonation reflection [2, 3, 7, 8]; they consequently identified that some aspects of the observed reflected shock conflict with what is predicted by ideal modeling. Inconsistencies were found in the post-reflected-shock pressure by Karnesky et al. [3, 9]. Bifurcation of the reflected shock was investigated as a possible explanation but was not observed in experiments [10, 11]. Damazo and Shepherd [12, 13] performed highly-resolved near-wall measurements of normal detonation reflection and found that the reflected shock speed was initially much larger than expected. It was proposed that upon reflecting into the incident detonation's induction zone, the twice-shocked reactants explode, driving a blast wave into the flow ahead, which results in the measurements of elevated shock speed near the wall [13]. The authors used a "square-wave" detonation model to demonstrate aspects of these dynamics, however further research was warranted to clarify the evolution of the near-wall reflected shock. The observation of anomalous reflected shock speeds illustrated that the ideal detonation assumed by modelers neglects important features of the underlying physics.

The purpose of the present work is to investigate the shock dynamics from normal reflection of finite thickness detonations by the analysis of numerical simulations. One-dimensional simulations of both supported and unsupported detonations are performed, where only in the latter case does the TZ form, and so its effects can be isolated. A one-gamma, one-step detonation model with reduced activation energy is used to simplify exact analysis of simulation results with methods that describe shock propagation through nonuniform flows. The theory is an extension to the shock-change equations, used previously to model ideal detonation reflection [6]. The derived equation describes shock acceleration caused by the equation's forcing, or source terms, which correspond to the net effects of flow gradients ahead of and behind the shock wave. The application of these methods to analyze simulation data enables clear conclusions to be drawn and explain the observed reflected shock acceleration. Results show that the reflected shock exhibits large near-wall acceleration, overshooting the speed predicted by reflecting the CJ state. The large shock acceleration is shown to be caused by shock propagation through the highly nonuniform flow in the incident detonation. The subsequent evolution of the shock depends on the detonation thickness relative to the pipe length. Simulations of unsupported detonations with varied pipe lengths illustrate how the finite detonation thickness affects the reflected shock's entire trajectory compared to predictions by simplified modeling. It is shown that for sufficiently short pipes, there is a transition in the type of reflected shock behavior, where the shock velocity increases monotonically until reaching the end of the TZ wave. Factors underlying all of the above reflected shock dynamics are discussed using the derived shock-change methods.

The structure of this article is as follows. In section 2, the problem of detonation reflection and the assumptions inherent in the methods used here are described. Numerical simulation methods and results are given in section 3. Methods to describe shock propagation through heterogeneous media are first derived in section 4.1 and then applied to the simulation results in section 4.2. Results from this study are further discussed in section 5.

2 Problem Formulation

Normal detonation reflection produces a shock that propagates through the incident detonation, hence treatment of the problem requires first a formulation of the incident detonation. Detonations are coupled combustion and shock waves that have been well established to be intrinsically multidimensional [14, 15] with significant influence from turbulence [16]. This is in contrast to normal shock waves that are exactly treated by one-dimensional and inviscid models. Even in one dimension, the coupling between chemical reaction and the shock front is well known to be highly unstable [17], resulting in an oscillating detonation speed, which leads to the cellular structure

observed in multidimensional detonations [18]. High levels of instability in the detonation front enables compressible turbulence to accelerate reactant burning and energy release [19]. The detonation front nonetheless exhibits periodicity such that a transverse or span-wise average describes mean quantities of a one-dimensional detonation like its speed and reaction zone structure. These mean structures may be treated using the highly-successful lower-dimensional and inviscid theories, however they are not equivalent. The models are only approximate but effective and useful for describing a transverse-mean detonation structure. Furthermore, although the one-dimensional detonation can be unstable, only a quasi-steady structure is considered important here.

The well-known classical theories describe the detonation speed, equilibrium thermodynamic state, reaction zone structure, and downstream flow. Chapman-Jouguet (CJ) theory predicts the detonation speed where chemical equilibrium coincides with a sonic point, terminating the detonation. The sonic point isolates the shock-driven combustion in the detonation, described by the Zel'dovich-Neumann-Döring (ZND) equations, from the downstream fluid dynamics. A zero-velocity downstream boundary condition, as is typical in pipes, requires an unsteady expansion, i.e., the TZ wave forms to bring the high-velocity combustion products to a halt. A piston boundary condition can instead match the combustion product velocity, so that no expansion wave forms. These two cases describe an unsupported and supported detonation, respectively.

In addition to only using one-dimensional analysis, a highly-simplified one-gamma one-step detonation model with reduced activation energy is used throughout this article. The reduced activation energy stabilizes the detonation [20], and the one-gamma one-step model enables straightforward analysis with theory, however as a consequence important characteristics of real chemical reaction mechanisms are lost. Because of the reduced activation energy, there is no considerable induction zone, and coupling between the post-reflected-shock thermodynamic state and reaction rate is weak. Damazo and Shepherd [13] discussed the possibility that prompt explosion of twice-shocked reactants behind the initially-frozen reflected shock may drive a substantially faster overdriven detonation in the incident detonation's induction zone. This possibility cannot be investigated using the present detonation model with reduced activation energy. Post-reflected-shock chemical reaction, subsequent energy release, and its effect to accelerate the reflected shock are considered here, however the results are particular to the single-step model and cannot be used to generalize for all cases of normal detonation reflection. Analysis of the general problem of detonation initiation in the incident detonation's induction zone and the ensuing dynamics remains for future research.

The incident detonation shock reflects and propagates first through the detonation's reaction zone structure, followed by the post-detonation flow. Propagation of the reflected shock wave through the unsupported detonation is diagrammed in Fig. 1, where after traversing the detonation itself the shock transmits into the TZ wave. The TZ wave is a self-similar centered expansion that scales with the distance the detonation has traveled. The one-dimensional solution for the TZ wave is well known [21]. Upon the detonation's collision with the wall, the TZ wave extends the entire length of the pipe. Hence, there are two essential length scales describing reflection of an unsupported detonation: a length scale describing the detonation thickness, Δ, and the length of the pipe, L. If the detonation thickness is much smaller than the pipe length such that $\Delta/L \to 0$, then all gradients at the detonation sonic point go to zero, and the detonation becomes supported. This shows that the supported detonation is a particular case or the limit of an unsupported detonation. Likewise, in the same limit, the influence of the detonation structure on the propagation of the reflected shock through the TZ wave is negligible, and the reflected shock can be approximated to have originated from reflection of the CJ state. This suggests that, in the limit of large pipe length, the reflected shock trajectory might be formulated as a boundary layer problem, where the outer problem describes the reflected shock propagation through the TZ wave, and the inner problem describes the shock's propagation through the detonation reaction zone. The outer problem has been modeled historically, as described above, where the convenient idealized detonation was used. Here we examine the inner problem, reflection of the supported detonation, and how the length scales in the unsupported detonation reflection affect the reflected shock's evolution.

An important consequence of the one-step detonation model is that the detonation is described only by a single length scale. Typically, with more detailed reaction mechanisms the ZND model exhibits two principle length scales: one describing the induction

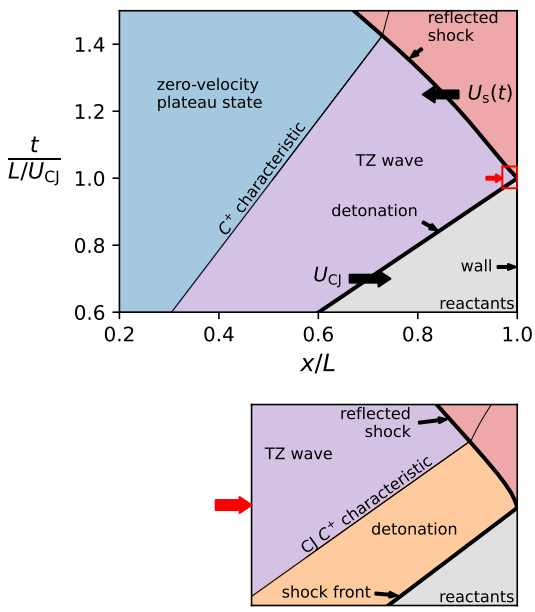

Fig. 1 Diagram of one-dimensional detonation reflection in a pipe of length, L. The detonation, traveling at the Chapman-Jouguet (CJ) speed, U_{CJ}, impacts the wall on the right, reflecting a shock wave that travels to the left. The reflected shock traverses the detonation itself followed by the Taylor-Zel'dovich (TZ) wave until it reaches the uniform zero-velocity plateau state behind the TZ wave

length, and a second describing the exothermic energy release length [15]. The single length scale in the present analysis allows the detonation thickness to be scaled unambiguously.

With a one-gamma detonation model, the perfect gas Rankine-Hugoniot equations can be solved to find useful preliminary results describing the relative shock speeds reflected by the von Neumann (vN) and CJ states. Upon impact with the wall, the initial speed of the reflected shock is such that the incident gas at the vN point is brought to rest by the reflected shock to match the zero-velocity boundary condition. If $\Delta/L \sim 0$, then after sufficient time for the shock to propagate into the equilibrium asymptote and for non-steady effects to vanish, the shock speed approaches a limit where the CJ state is brought to rest. The magnitude of these two shock speeds can be obtained exactly for the one-gamma detonation. The vN reflected shock speed, $U_{\mathrm{s,vN}}$, is given by

$$\frac{U_{\mathrm{s,vN}}}{U_{\mathrm{CJ}}} = \frac{1}{M_{\mathrm{CJ}}^2}\left(1 + 2\frac{\gamma-1}{\gamma+1}(M_{\mathrm{CJ}}^2 - 1)\right) , \quad (1)$$

and the CJ reflected shock speed, $U_{\mathrm{s,CJ}}$, is given by

$$\frac{U_{\mathrm{s,CJ}}}{U_{\mathrm{CJ}}} = \frac{\gamma-3}{4}\frac{M_{\mathrm{CJ}}^2-1}{(\gamma+1)M_{\mathrm{CJ}}^2} + \frac{1}{M_{\mathrm{CJ}}^2}\sqrt{\left(\frac{M_{\mathrm{CJ}}^2-1}{4}\right)^2 + \left(\frac{\gamma M_{\mathrm{CJ}}^2+1}{\gamma+1}\right)^2} , \quad (2)$$

where U_{CJ} and M_{CJ} are the CJ speed and Mach number, respectively. These are shock speeds in the laboratory-fixed frame, and γ is the ratio of specific heat capacities.

The ratio of these two reflected shock speeds is plotted for $1 < \gamma < 5/3$ and select CJ Mach numbers in Fig. 2. The ratio illustrates that for a gas the shock speed ratio is always less than unity, i.e. the vN reflected shock is always slower than the CJ reflected shock. Since the reflected shock always originates from the vN point, the reflected shock must accelerate in order to reach the asymptotic CJ reflected shock speed.

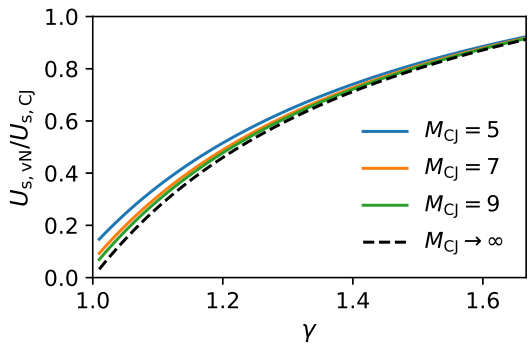

Fig. 2 Ratio of vN and CJ reflected shock speeds for a one-gamma detonation

The ratio of vN and CJ reflected shock speeds is also plotted for the strong detonation approximation in Fig. 2, where the ratio is given by

$$\frac{U_{\mathrm{s,vN}}}{U_{\mathrm{s,CJ}}} \approx \frac{8(\gamma-1)}{\gamma - 3 + \sqrt{1+\gamma(17\gamma+2)}} , \quad (3)$$

and the ratio only equals unity when

$$\gamma = \frac{9+\sqrt{33}}{8} \approx 1.84 . \quad (4)$$

For the one-gamma detonation model used in this article with $\gamma = 1.2$ and $M_{\mathrm{CJ}} = 7$, the vN and CJ reflected shock speeds are, respectively,

$$\begin{aligned} \frac{U_{\mathrm{s,vN}}}{U_{\mathrm{CJ}}} &= 0.20 \\ \frac{U_{\mathrm{s,CJ}}}{U_{\mathrm{CJ}}} &= 0.41 \ . \end{aligned} \tag{5}$$

3 Numerical Simulations

3.1 Methods

Direct simulation of the one-dimensional reactive Euler equations was performed using the finite-volume CFD toolbox, OpenFOAM-9 [22], with the additional library blastFoam-5 [23].

A one-gamma, one-step detonation model was used for all simulations. An Arrhenius rate law was used for the single first-order irreversible reaction. The reaction equation, rate constant, and enthalpy are given by

$$\begin{aligned} R &\rightarrow P \\ k(T) &= A \exp(-T_{\mathrm{a}}/T) \\ h_R &= c_P T \\ h_P &= c_P T - Q \ , \end{aligned} \tag{6}$$

where R and P are reactant and product species, respectively, h_R and h_P are their respective enthalpies, c_P is the specific heat capacity at constant pressure, T_{a} is the activation temperature, A is the pre-exponential factor, and Q is the energy release. The energy release was specified in the one-gamma detonation through the CJ Mach number with $M_{\mathrm{CJ}} = 7$ [24]. The gamma or ratio of specific heats chosen was $\gamma = 1.2$. Although these values for the CJ Mach number and gamma are typical, the parameters are chosen for convenience and not to replicate the properties for a particular mixture.

In order to simulate stable unsupported detonations, a reduced activation energy, $T_{\mathrm{a}}/T_{\mathrm{vN}} = 3$, was used, where T_{vN} is the temperature at the von Neumann point. The reduced activation energy substantially decouples the reaction rate from the post-shock thermodynamics, which eliminates instabilities [20] at a cost of limiting the generality of results, as discussed in section 2.

The rate law pre-exponential constant was used to scale the ZND reaction zone size, which was taken to be the half-reaction-zone thickness, $\Delta_{1/2}$, which is the width of the ZND reaction zone where the reaction progress variable equals one half. The ZND reaction zone structure for this one-gamma, one-step detonation model is shown in Fig. 3.

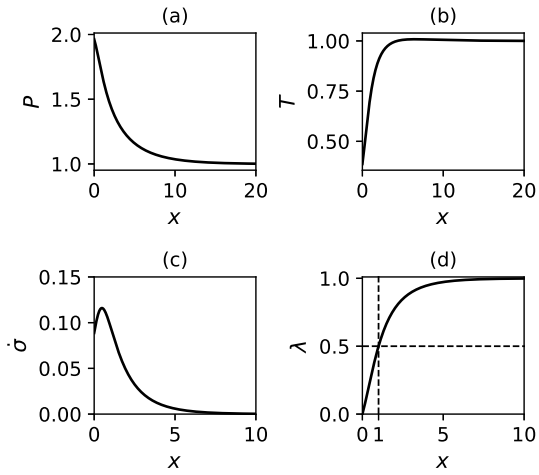

Fig. 3 ZND reaction zone structure for one-gamma, one-step detonation model with $\gamma = 1.2$, $M_{\mathrm{CJ}} = 7$, $T_{\mathrm{a}}/T_{\mathrm{vN}} = 3$, and scaled by half-reaction-zone width, $\Delta_{1/2}$. Quantities shown are (a) pressure, (b) temperature, (c) thermicity, and (d) reaction progress variable, with all appropriately nondimensionalized by the CJ state

The one-step reaction mechanism was constructed and implemented first in Cantera [25] using the techniques described by Kao [26]. Thermodynamics are computed in both Cantera and OpenFOAM using NASA-7 polynomials [27]. The single irreversible reaction was translated to OpenFOAM's native units using the appropriate conversion factors. The ZND equations were solved using the routines in the Shock and Detonation Toolbox [28]. The temperature, pressure, lab-frame velocity, and reaction progress variable corresponding to the ZND solution were used to prescribe the initial condition for all simulations in OpenFOAM. The relevant initial condition and boundary conditions for the supported and unsupported detonation simulations are discussed in greater detail below.

For all simulations, a rightward propagating detonation is considered such that the detonation impacts the right domain wall and reflects a shock wave to the left. However, simulation results are flipped to describe rightward reflected shock propagation with positive lab-frame shock speeds.

For unsupported detonation simulations, results for the reflected shock trajectory are compared with

those given by the idealized model with an infinitesimal detonation thickness. The specific model used is the one described by Schoeffler and Shepherd [6], where a shock-change equation is integrated assuming that the post-reflected-shock velocity gradient is uniform.

Simulation data were post-processed to compute the reflected shock position, velocity, and relevant pre-shock and post-shock quantities. An algorithm was implemented to consistently extract these quantities by fitting the upstream and downstream flows bounding the shock. The finite volume solver generates shocks that are approximately five cells thick. At each saved time step, the maximum derivative of the pressure data was used to initially locate the shock wave. Using the pressure data, the shock wave, the immediate upstream flow, and the immediate downstream flow were each fitted to lines. Twenty grid points were used to fit the upstream and downstream flows, respectively, except when the shock was near the wall, where the known shock thickness was used to approximate the upstream and downstream coordinates. Using additional grid points in fitting the upstream and downstream flows introduces nonuniformity in fit residuals resulting from nonuniform flow gradients, which would require higher-order polynomials to properly fit. Since only the immediate upstream and downstream states were of interest, the linear fit to twenty grid points was found to be adequate for evaluating these states and the velocity gradient. The two intersection points between the shock-fitted line and the upstream and downstream lines were used as coordinates for the pre-shock and post-shock states, respectively. The position of the shock was taken to be the average of these two points. All other pre-shock and post-shock quantities were then computed by interpolating simulation data at these coordinates. An example of the results of this post-processing algorithm is shown in Fig. 4.

The shock velocity was computed by numerically differentiating the position data. The post-shock velocity gradient was extracted from the slope of the line fitted to the downstream flow velocity. The time-derivative of pre-shock quantities was also computed by numerical differentiation.

All results presented below are nondimensional using the following normalizations for pressure, P, temperature, T, density, ρ, velocity, u, time, t, and

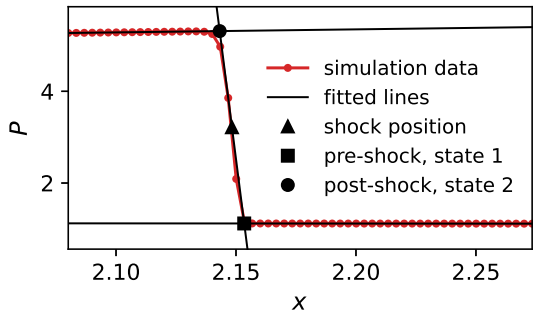

Fig. 4 Diagram of numerical shock features captured by post-processing algorithm. Pressure is plotted, normalized by the CJ pressure, against the spatial coordinate, normalized by the half-reaction-zone width, $\Delta_{1/2}$

distance, x,

$$P = \frac{\tilde{P}}{\tilde{P}_{\mathrm{CJ}}}, \quad T = \frac{\tilde{T}}{\tilde{T}_{\mathrm{CJ}}}, \quad \rho = \frac{\tilde{\rho}}{\tilde{\rho}_{\mathrm{CJ}}}, \\ u = \frac{\tilde{u}}{\tilde{U}_{\mathrm{CJ}}}, \quad t = \frac{\tilde{t}}{\tilde{t}_{\mathrm{ref}}}, \quad x = \frac{\tilde{x}}{\tilde{\Delta}_{1/2}}, \tag{7}$$

where the tilde identifies dimensional variables, the subscript CJ refers to the CJ state, and the reference time scale is

$$\tilde{t}_{\mathrm{ref}} = \frac{\tilde{\Delta}_{1/2}}{\tilde{U}_{\mathrm{CJ}}} \, . \tag{8}$$

Note that the velocity normalization uses the CJ speed, $\tilde{U}_{\mathrm{CJ}}$, and not the gas velocity at the CJ state.

3.2 Simulation of Supported Detonation Reflection

3.2.1 Simulation Details

Reflection of a supported detonation was simulated by initializing the ZND reaction zone structure with shock front coincident with end wall. The right domain boundary is chosen to be the reflecting wall with a zero-velocity boundary condition. The equilibrium asymptote of the ZND model, i.e., the CJ state, is extended to a sufficient domain length for the reflected shock to propagate. The domain length chosen was $L = 80$. The prescribed initial condition for the simulation is shown in Fig. 5.

Zero-gradient boundary conditions are used for all other quantities, including the left domain wall velocity. The grid resolution was 300 cells per $\Delta x = 1$ (i.e., 300 cells per $\Delta_{1/2}$), and time steps are saved every $\Delta t = 0.077$.

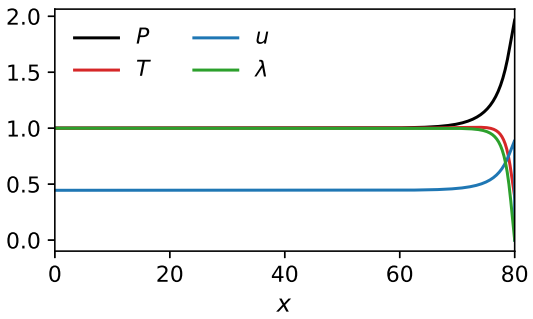

Fig. 5 Initial conditions for simulation of supported detonation reflection. The von Neumann point is located at the right wall

3.2.2 Simulation Results

Near-wall evolution of the pressure and lab-frame velocity are plotted in Fig. 6. Fig. 6(a) shows a rapid decrease in post-shock pressure as the left-running shock wave accelerates away from the wall. Fig. 6(b) shows that the velocity of the post-shock flow is negative with an approximately constant gradient between the post-shock state to the zero-velocity boundary condition.

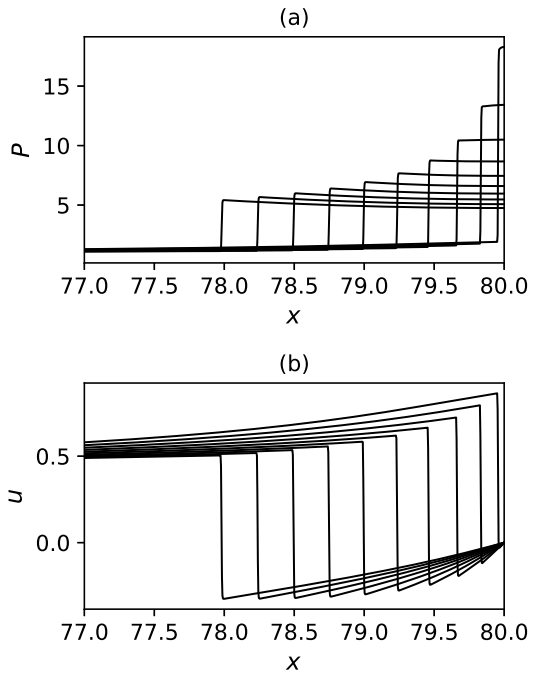

Fig. 6 Near-wall evolution of pressure and lab-frame velocity from reflected shock wave propagation. The wall is at $x = 80$. The time difference between each plot is $\Delta t = 0.34$

The velocity of the reflected shock wave is plotted over time in Fig. 7. The velocity is initially equal to the shock speed reflected by the von Neumann point, which is $U_{\mathrm{s,vN}} = 0.20$. As the reflected shock propagates away from the wall, it rapidly accelerates and overshoots the CJ reflection limit, $U_{\mathrm{s,CJ}} = 0.41$. The shock speed reaches a maximum velocity of $U_{\mathrm{s}} = 0.67$ at time $t = 3.96$ and position $X_{\mathrm{s}} = 2.23$. The shock speed subsequently decays over a substantially longer time, first reaching the CJ reflection asymptote at time $t = 77.6$ and position $X_{\mathrm{s}} = 37.5$. The shock decays slightly below the CJ reflection asymptote to a minimum of $U_{\mathrm{s}} = 0.40$ at time $t = 116.5$, before accelerating again toward the asymptote.

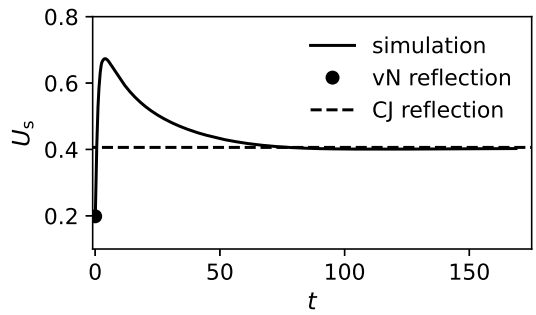

Fig. 7 Lab-frame reflected shock speed from supported detonation reflection

Although the shock wave achieves a large peak in lab-frame velocity, the shock Mach number, plotted in Fig. 8, is at a maximum initially and then decays to the CJ reflection limit. The initial decay of the shock Mach number is very rapid and then subsequently slower. The shock Mach number first decays below the CJ reflection limit, before slowly increasing toward the limit.

The effect of the shock acceleration is to displace the space-time trajectory of the shock relative to the straight-line trajectory of a shock traveling at the CJ reflection speed, as shown in Fig. 9. The magnitude of this displacement, δx, is given by integrating the difference between the reflected shock velocity and the CJ reflection limiting value, i.e.,

$$\delta x = \int_0^{t_{\mathrm{f}}} U_{\mathrm{s}}(t) - U_{\mathrm{s,CJ}} \, \mathrm{d}t \, , \tag{9}$$

where t_{f} is the end of the simulation. Integrating the simulation data yields $\delta x = 5.55$. The significance of

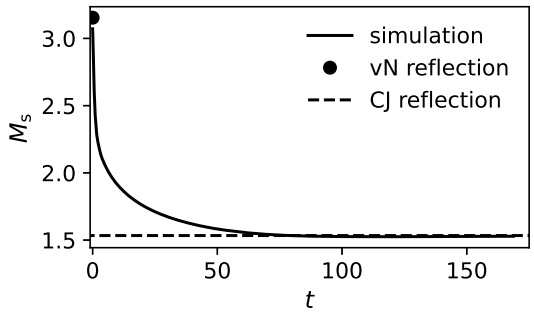

Fig. 8 Shock Mach number of reflected shock from supported detonation reflection

this displacement is that it manifests as a kinked space-time diagram when time-of-arrival measurements are used in experiments to examine the shock's trajectory, as illustrated by Damazo and Shepherd [13].

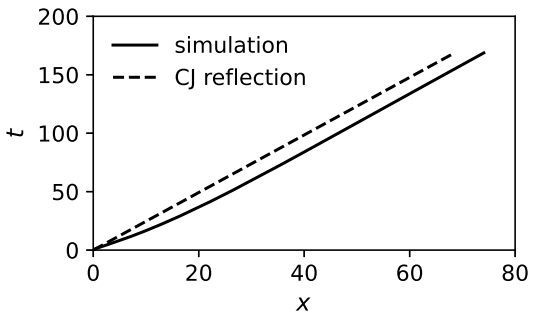

Fig. 9 Space-time diagram for reflected shock from supported detonation simulation compared with constant shock speed from CJ reflection

The pressure-transient at the end wall is plotted in Fig. 10. The pressure is initially very large, although the simulation does not quite resolve the vN reflection pressure. Similar to the shock speed and Mach number, the pressure decays slightly below the CJ reflection limit, before increasing toward it. The pressure first intersects the CJ reflection limit at time $t = 16.4$. Because of the finite detonation thickness there is an excess impulse exerted on the pipe end wall, which can be found from the integral,

$$\frac{I_\mathrm{e}}{A} = \int_0^{t_\mathrm{f}} P_\mathrm{wall}(t) - P_\mathrm{r,CJ}\ \mathrm{d}t = 26.8\ , \tag{10}$$

$$\frac{\tilde{I}_\mathrm{e}}{\tilde{A}} = 26.8\frac{\tilde{P}_\mathrm{CJ}\tilde{\Delta}_{1/2}}{\tilde{U}_\mathrm{CJ}}\ , \tag{11}$$

where I_e is the excess impulse, A is the end wall area, P_wall is the pressure at the end wall, and $P_\mathrm{r,CJ}$ is the CJ reflection pressure. The dimensional impulse is also given in (11) to make the scaling explicit. The vast majority of this excess impulse is exerted during the initial decay from the peak pressure, i.e., over time $t = 16.4$. This impulse increment is in addition to the impulse exerted by CJ reflection, and, in general, the impulse exerted by detonation reflection continues to increase monotonically with time [29].

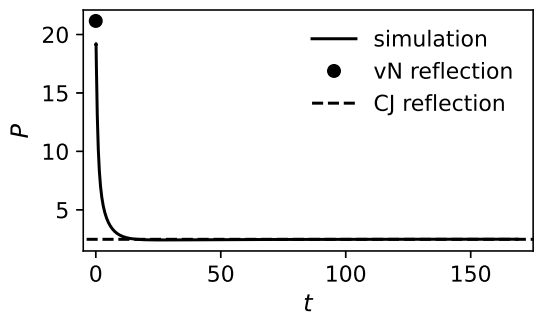

Fig. 10 End-wall pressure over time following supported detonation reflection

3.3 Simulation of Unsupported Detonation Reflection

3.3.1 Simulation Details

An unsupported detonation was simulated by initializing a width of the ZND model for a rightward propagating detonation at the left domain wall, so that upon simulating the wave's evolution a zero-velocity boundary condition at the left domain wall generates the TZ wave as the detonation propagates. The width of the ZND model chosen was $5\Delta_{1/2}$. An initial kink in the propagating detonation between the reaction zone and TZ wave smooths as the detonation propagates. The evolution of this initial condition is illustrated in Fig. 11. Zero-gradient boundary conditions are used for all other quantities. The grid resolution was 200 cells per $\Delta x = 1$ (i.e., 200 cells per $\Delta_{1/2}$), and time steps are sampled every $\Delta t = 0.154$.

The unsupported detonation exhibits two length scales: a length scale for the detonation thickness, here $\Delta_{1/2}$, and the domain length scale, L. Unsupported detonation reflection was simulated for four domain lengths, $L = 50$, 100, 200, and 500. All simulations

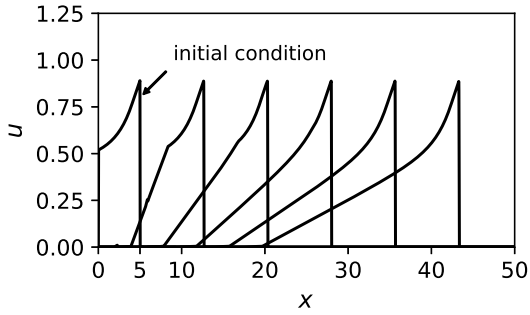

Fig. 11 Velocity initial condition and its evolution for unsupported detonation. $\Delta t = 7.67$ between curves

begin with the same initial condition, such that by extending the length of the domain the same detonation is allowed to propagate further. Fig. 12 shows the detonation pressure data just before the wave reaches the domain end wall for the four simulation cases.

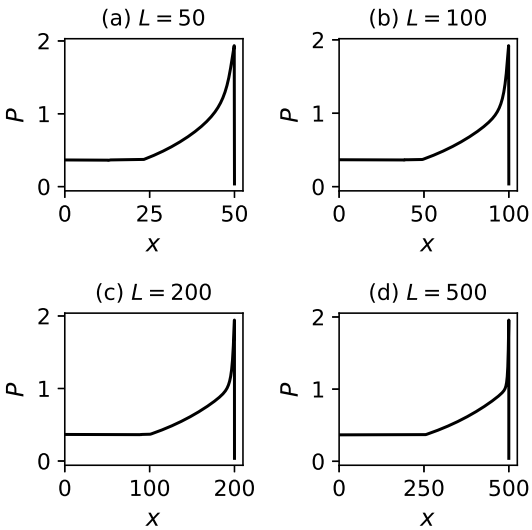

Fig. 12 Pressure data of unsupported detonation before impacting right domain wall for four domain lengths

3.3.2 Simulation Results

Because there are two intrinsic length scales in this problem, the simulation results are plotted using both scales. Scaling by the reaction zone thickness describes reflection of a given detonation in multiple pipe lengths. Scaling by the domain length illustrates how a varied detonation thickness produces different reflected shock dynamics in a fixed length detonation tube. When scaling by the domain length, the coordinates in space and time are divided by the nondimensional domain length, for example, time is given by

$$\frac{t}{L} = \frac{\tilde{t}\tilde{U_{\mathrm{CJ}}}}{\tilde{\Delta}_{1/2}} \frac{\tilde{\Delta}_{1/2}}{\tilde{L}} \,. \tag{12}$$

Results are only compared with the ideal model when using the domain length scale, since the ideal model only exists for an infinitesimal detonation thickness.

The reflected shock velocity is plotted over time for the four domain lengths in Fig. 13. For all cases, the shock velocity is initially equal to the velocity of the shock reflected by the von Neumann point. Fig. 13(a) shows that all reflected shocks exhibit a period of rapid acceleration near the wall, which is indistinguishable between the cases up until some point in time. The subsequent dynamics vary distinctly between the different simulated domain lengths. At a later point in time, the shock trajectories for all cases feature a local velocity maximum. This peak corresponds to the reflected shock's arrival in the zero-velocity plateau state that exists behind the TZ wave. In this region, all shocks begin to decay, hence the maxima in shock velocity. The reflected shock behavior between these two points, the early point where trajectories first diverge and the later point where all shocks reach the end of the TZ wave, is substantially different. For the shorter domain length cases, $L = 50$ and 100, the reflected shock velocity increases monotonically until reaching the end of the TZ wave. For the longer domain length cases, $L = 200$ and 500, the reflected shock velocity exhibits both a local maximum and minimum before the shock proceeds to accelerate through the TZ wave.

The shock velocity trajectories are shown in Fig. 13(b) with time scaled by the domain length. As the detonation thickness shrinks relative to a fixed domain length, the shock velocity begins to approach the ideal model with the exception of an early overshoot resulting from the finite detonation thickness.

A consequence of these dynamics is that as the domain length decreases, the maximum velocity achieved by the reflected shock increases. The maximum shock velocity, which coincides with the shock's arrival at the end of the TZ wave, is plotted in Fig. 14 for each domain length.

The space-time trajectories for the four simulation cases are plotted with the ideal model in Fig. 15. The trajectories are only shown up until the shock reaches

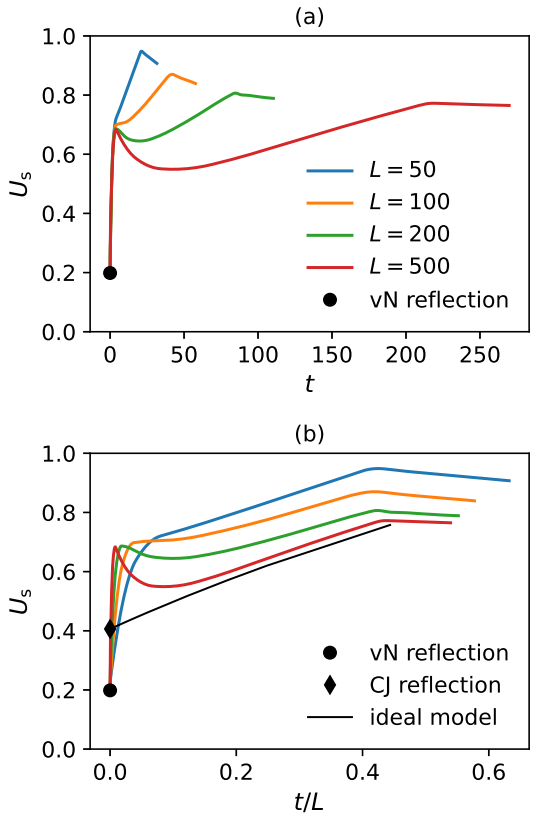

Fig. 13 Lab-frame reflected shock velocity from unsupported detonation for varied domain length plotted against time, scaled by reaction zone thickness in (a) and scaled by domain length in (b)

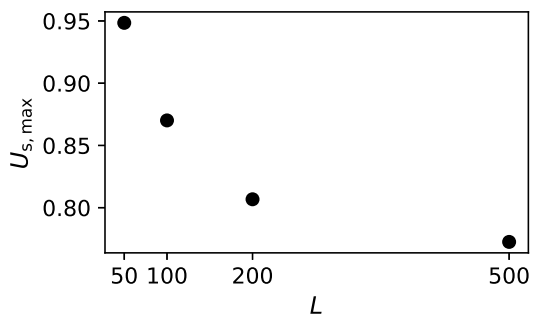

Fig. 14 Maximum reflected shock velocity from unsupported detonation reflection

the end of the TZ wave. Again, as the detonation thickness shrinks the shock trajectory approaches the ideal model.

Pressure at the detonation-reflecting end wall is plotted over time for both scales in Fig. 16. Again,

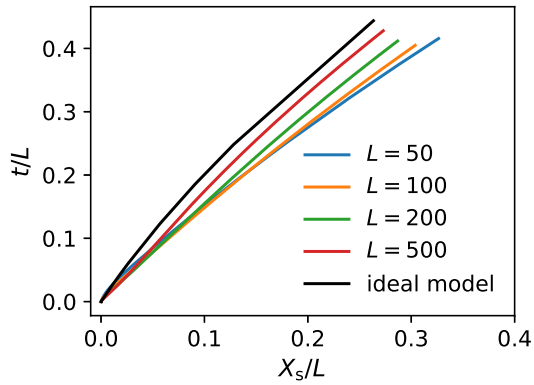

Fig. 15 Space-time trajectories of reflected shock from unsupported detonation for four domain lengths. All trajectories are terminated where the reflected shock arrives at the end of the TZ wave

the simulation results do not quite capture the initial vN reflection pressure. In all cases, the pressure decays monotonically. Fig. 16(a) shows that, as the reflected shock propagates through the reaction zone, the pressure decay is nearly indistinguishable between the different cases, and the subsequent decay as the shock propagates through the TZ wave scales with the length of the domain. Fig. 16(b) illustrates how a thicker detonation for a given detonation tube length increases the duration of the pressure pulse at the end wall. The excess impulse exerted against the end wall resulting from the finite detonation thickness is approximately equivalent to the result from simulation of the supported detonation.

4 Shock-Change Analysis

Analysis of the numerical simulation results requires methods that describe shock propagation through nonuniform upstream media. Shock propagation theories have been developed by numerous authors over many decades. A common technique is to consider the transport of shock-jump quantities, enabling a combination of the Euler equations with the Rankine-Hugoniot equations. The formalism, sometimes referred to as singular surface theory [30, 31], enables derivation of equations referred to by several names including shock-propagation and shock-amplitude equations, however, in detonation physics, they are most often known as the shock-change equations, as presented by Fickett and Davis [14]. There have been many contributions to the methods, some include those by Chen and Gurtin [32], Bowen

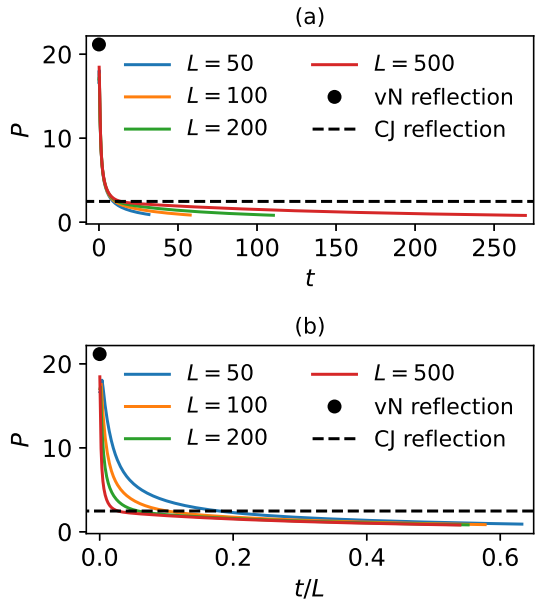

Fig. 16 End-wall pressure plotted over time following unsupported detonation reflection

and Chen [33], Nunziato and Kennedy [34, 35], and most recently by Radulescu [36, 37].

Shock propagation into nonuniform media has also been examined by several authors, however shock-change methods have typically only been used for uniform upstream flows. A notable exception is the work by Nunziato and Walsh [38–40]. Other methods were developed by Chisnell [5], and later generalized by Strachan et al. [4], to describe shock acceleration from upstream gradients by neglecting nonsteady influences behind the shock wave. The propagation of two-dimensional wave fronts through regions of nonuniformity has been treated with extensions to Whitham's theory [41], for example by Collins and Chen [42] and Catherasoo and Sturtevant [43, 44].

Methods using shock-change equations are distinct because they provide an exact description of how shock propagation is affected by upstream and downstream flow gradients. However, the gradients must be known *a priori* in order to make predictions of shock trajectories. To use the equations to compute shock evolution additional models are required and, although inexact, can yield highly accurate results [6, 37]. Methods have been developed to make higher-order approximations, as described by Best [45] and Sharma and Radha [30].

A powerful application of the shock-change equations is instead to use them to analyze simulation or experiment data, and this is the strategy we are taking here. The appropriate shock-change equation describing shock propagation through a nonuniform flow is first derived generally and then specified for a one-gamma perfect gas. The result is an ordinary differential equation for the shock velocity, which makes explicit how shock acceleration originates from forcing terms in the equation that describe the influence of flow gradients both ahead of and behind the shock wave.

4.1 Derivation of Shock-Change Equation

The equations of motion for a chemically reacting flow in one dimension, neglecting diffusion of mass, momentum, and heat, are

$$\frac{\mathrm{D}\rho}{\mathrm{D}t} = -\rho\frac{\partial u}{\partial x} \tag{13}$$

$$\frac{\mathrm{D}u}{\mathrm{D}t} = -\frac{1}{\rho}\frac{\partial P}{\partial x} \tag{14}$$

$$\frac{\mathrm{D}h}{\mathrm{D}t} = \frac{1}{\rho}\frac{\mathrm{D}P}{\mathrm{D}t} \tag{15}$$

$$\frac{\mathrm{D}Y_i}{\mathrm{D}t} = \frac{1}{\rho}W_i\dot{\omega}_i \qquad (i = 1, \ldots, N) \tag{16}$$

where species i has mass fraction Y_i, molecular weight W_i, and net production rate $\dot{\omega}_i$. An equation of state of the form $h = h(P, \rho, \mathbf{Y})$ can be expanded as

$$\mathrm{d}h = \left(\frac{\partial h}{\partial \rho}\right)_{P,\mathbf{Y}} \mathrm{d}\rho + \left(\frac{\partial h}{\partial P}\right)_{\rho,\mathbf{Y}} \mathrm{d}P + \sum_{k=1}^{N}\left(\frac{\partial h}{\partial Y_k}\right)_{\rho,P,Y_{i\neq k}} \mathrm{d}Y_k\,, \tag{17}$$

where $\mathbf{Y}$ is a vector containing the N species mass fractions.

Expressing the total differentials in (17) as material derivatives and combining with (15) gives

$$\left(\frac{1}{\rho} - \left(\frac{\partial h}{\partial P}\right)_{\rho,\mathbf{Y}}\right)\frac{\mathrm{D}P}{\mathrm{D}t} = \left(\frac{\partial h}{\partial \rho}\right)_{P,\mathbf{Y}}\frac{\mathrm{D}\rho}{\mathrm{D}t} + \sum_{k=1}^{N}\left(\frac{\partial h}{\partial Y_k}\right)_{\rho,P,Y_{i\neq k}}\frac{\mathrm{D}Y_k}{\mathrm{D}t}. \tag{18}$$

After further manipulation, the following result is obtained

$$\frac{\mathrm{D}P}{\mathrm{D}t} = a_\mathrm{f}^2 \frac{\mathrm{D}\rho}{\mathrm{D}t} + \rho a_\mathrm{f}^2 \dot{\sigma} \tag{19}$$

where a_f is the frozen sound speed [46],

$$a_\mathrm{f}^2 = \frac{\left(\dfrac{\partial h}{\partial \rho}\right)_{P,\mathbf{Y}}}{\dfrac{1}{\rho} - \left(\dfrac{\partial h}{\partial P}\right)_{\rho,\mathbf{Y}}} , \tag{20}$$

and $\dot{\sigma}$ is the thermicity,

$$\dot{\sigma} = -\frac{\beta}{c_P} \sum_{k=1}^{N} \left(\frac{\partial h}{\partial Y_k}\right)_{\rho,P,Y_{i\neq k}} \frac{\mathrm{D}Y_k}{\mathrm{D}t} . \tag{21}$$

β is the coefficient of thermal expansion, and c_P is the specific heat capacity at constant pressure.

The result (19) is well known and sometimes referred to as the adiabatic-change equation [14]. It can be used to eliminate the material derivative of density from the continuity equation (13),

$$\frac{\mathrm{D}P}{\mathrm{D}t} = -\rho a_\mathrm{f}^2 \frac{\partial u}{\partial x} + \rho a_\mathrm{f}^2 \dot{\sigma}, \tag{22}$$

resulting in a system of two equations with the momentum equation (14).

Fluid elements travel with velocity u relative to a consistent reference frame, often termed the laboratory-fixed frame. The time variation of flow quantities, such as pressure, density, and velocity, along particle paths is described by the material derivative. Similarly, the time variation of flow quantities along the path of a shock wave can be computed with the corresponding total derivative. An arbitrary field quantity, $q = q(x,t)$, evaluated along the path of a shock wave is given by $q = q(X_\mathrm{s}(t), t)$, where $X_\mathrm{s}(t)$ is the position of the shock wave. Then, the time variation of q along the path of the shock is

$$\left.\frac{\mathrm{d}q}{\mathrm{d}t}\right|_\mathrm{s} = \frac{\partial q}{\partial t} + \frac{\mathrm{d}X_\mathrm{s}}{\mathrm{d}t}\frac{\partial q}{\partial x} = \frac{\partial q}{\partial t} + U_\mathrm{s}\frac{\partial q}{\partial x} , \tag{23}$$

where U_s is the lab-frame shock velocity. The time derivative of a quantity along the path of the shock will be subsequently referred to as the quantity's *shock derivative*.

The material derivative can be written in terms of the shock derivative with

$$\frac{\mathrm{D}q}{\mathrm{D}t} = \left.\frac{\mathrm{d}q}{\mathrm{d}t}\right|_\mathrm{s} + (u - U_\mathrm{s})\frac{\partial q}{\partial x} , \tag{24}$$

which can be used to transform (14) and (22). This change of variables gives

$$\left.\frac{\mathrm{d}u}{\mathrm{d}t}\right|_\mathrm{s} + (u - U_\mathrm{s})\frac{\partial u}{\partial x} = -\frac{1}{\rho}\frac{\partial P}{\partial x} \tag{25}$$

$$\left.\frac{\mathrm{d}P}{\mathrm{d}t}\right|_\mathrm{s} + (u - U_\mathrm{s})\frac{\partial P}{\partial x} = -\rho a_\mathrm{f}^2 \frac{\partial u}{\partial x} + \rho a_\mathrm{f}^2 \dot{\sigma} . \tag{26}$$

Equations (25) and (26) can be combined to either eliminate the pressure-gradient term or the velocity-gradient term to arrive at a shock-change equation. Here we consider only the velocity gradient and eliminate the pressure gradient, and the corresponding shock-change equation is

$$\left.\frac{\mathrm{d}P_2}{\mathrm{d}t}\right|_\mathrm{s} + \rho_2 w_2 \left.\frac{\mathrm{d}u_2}{\mathrm{d}t}\right|_\mathrm{s} = \rho_2 a_{\mathrm{f},2}^2 \left(\dot{\sigma} - \eta \left.\frac{\partial u}{\partial x}\right|_2\right) \tag{27}$$

where the η is the sonic parameter,

$$\eta = 1 - \frac{w_2^2}{a_{\mathrm{f},2}^2}, \tag{28}$$

and $w_2 = U_\mathrm{s} - u_2$ is the flow velocity in the shock-fixed frame. The subscript 2 was also introduced to indicate that the variables are post-shock quantities, whereas a subscript 1 refers to a pre-shock or upstream quantity. The subscripts make explicit the relationship between the shock-change equations and the shock-jump equations, which describe how state 1 quantities are related to state 2 quantities. The relevant Rankine-Hugoniot or shock-jump relations can be expressed as

$$P_2 = P_2(U_\mathrm{s}, u_1, P_1, \rho_1, \mathbf{Y_1}) \tag{29}$$

$$u_2 = u_2(U_\mathrm{s}, u_1, P_1, \rho_1, \mathbf{Y_1}) , \tag{30}$$

i.e., the post-shock pressure and velocity are functions of the shock speed, the upstream flow velocity, and the upstream thermodynamic state. The thermodynamic state is here defined by the set of independent variables $\{P, \rho, \mathbf{Y}\}$, however any equivalent set can be used.

The shock derivatives in (27) can be evaluated by differentiating the shock-jump relations, (29) and (30). By applying the chain rule, the shock derivatives of post-shock pressure and velocity are given in terms of the shock acceleration and the shock derivatives of upstream quantities.

If the upstream flow is nonuniform, then generally each term in (29) and (30) can be an independent function of time, and so the chain rule must be applied to each term. The expansion of (29) is

$$\begin{aligned}\left.\frac{\mathrm{d}P_2}{\mathrm{d}t}\right|_\mathrm{s} = &\left.\frac{\partial P_2}{\partial U_\mathrm{s}}\right|_{u_1,P_1,\rho_1,\mathbf{Y_1}} \left.\frac{\mathrm{d}U_\mathrm{s}}{\mathrm{d}t}\right|_\mathrm{s} \\ &+\left.\frac{\partial P_2}{\partial u_1}\right|_{U_\mathrm{s},P_1,\rho_1,\mathbf{Y_1}} \left.\frac{\mathrm{d}u_1}{\mathrm{d}t}\right|_\mathrm{s} \\ &+\left.\frac{\partial P_2}{\partial P_1}\right|_{U_\mathrm{s},u_1,\rho_1,\mathbf{Y_1}} \left.\frac{\mathrm{d}P_1}{\mathrm{d}t}\right|_\mathrm{s} \\ &+\left.\frac{\partial P_2}{\partial \rho_1}\right|_{U_\mathrm{s},u_1,P_1,\mathbf{Y_1}} \left.\frac{\mathrm{d}\rho_1}{\mathrm{d}t}\right|_\mathrm{s} \\ +\sum_{k=1}^{N} &\left.\frac{\partial P_2}{\partial Y_{1,k}}\right|_{U_\mathrm{s},u_1,\rho_1,P_1,\mathbf{Y_{1,i\neq k}}} \left.\frac{\mathrm{d}Y_{1,k}}{\mathrm{d}t}\right|_\mathrm{s}\end{aligned} \tag{31}$$

where the subscripted terms keep track of those that are held constant during the partial differentiation. The upstream flow velocity in the shock-fixed frame is $w_1 = U_\mathrm{s} - u_1$ and can be used to simplify the partial-derivative terms, which gives

$$\begin{aligned}\left.\frac{\mathrm{d}P_2}{\mathrm{d}t}\right|_\mathrm{s} = &\left.\frac{\partial P_2}{\partial w_1}\right|_{P_1,\rho_1,\mathbf{Y_1}} \left.\frac{\mathrm{d}U_\mathrm{s}}{\mathrm{d}t}\right|_\mathrm{s} \\ &-\left.\frac{\partial P_2}{\partial w_1}\right|_{P_1,\rho_1,\mathbf{Y_1}} \left.\frac{\mathrm{d}u_1}{\mathrm{d}t}\right|_\mathrm{s} \\ &+\left.\frac{\partial P_2}{\partial P_1}\right|_{w_1,\rho_1,\mathbf{Y_1}} \left.\frac{\mathrm{d}P_1}{\mathrm{d}t}\right|_\mathrm{s} \\ &+\left.\frac{\partial P_2}{\partial \rho_1}\right|_{w_1,P_1,\mathbf{Y_1}} \left.\frac{\mathrm{d}\rho_1}{\mathrm{d}t}\right|_\mathrm{s} \\ +\sum_{k=1}^{N} &\left.\frac{\partial P_2}{\partial Y_{1,k}}\right|_{w_1\rho_1,P_1,\mathbf{Y_{1,i\neq k}}} \left.\frac{\mathrm{d}Y_{1,k}}{\mathrm{d}t}\right|_\mathrm{s} .\end{aligned} \tag{32}$$

Each partial-derivative coefficient in (32) is a partial derivative of the instantaneous shock Hugoniot, i.e., each coefficient is only a function of the instantaneous shock velocity and upstream state. With the specification of an equation of state, each partial-derivative coefficient can be calculated by suitably differentiating the Rankine-Hugoniot relations.

The chain-rule expansion for the shock derivative of the lab-frame velocity (30) is

$$\begin{aligned}\left.\frac{\mathrm{d}u_2}{\mathrm{d}t}\right|_\mathrm{s} = &\left.\frac{\mathrm{d}U_\mathrm{s}}{\mathrm{d}t}\right|_\mathrm{s} - \left.\frac{\partial w_2}{\partial w_1}\right|_{P_1,\rho_1,\mathbf{Y_1}} \left.\frac{\mathrm{d}U_\mathrm{s}}{\mathrm{d}t}\right|_\mathrm{s} \\ &+\left.\frac{\partial w_2}{\partial w_1}\right|_{P_1,\rho_1,\mathbf{Y_1}} \left.\frac{\mathrm{d}u_1}{\mathrm{d}t}\right|_\mathrm{s} \\ &-\left.\frac{\partial w_2}{\partial P_1}\right|_{w_1,\rho_1,\mathbf{Y_1}} \left.\frac{\mathrm{d}P_1}{\mathrm{d}t}\right|_\mathrm{s} \\ &-\left.\frac{\partial w_2}{\partial \rho_1}\right|_{w_1,P_1,\mathbf{Y_1}} \left.\frac{\mathrm{d}\rho_1}{\mathrm{d}t}\right|_\mathrm{s} \\ -\sum_{k=1}^{N} &\left.\frac{\partial w_2}{\partial Y_{1,k}}\right|_{w_1,\rho_1,P_1,\mathbf{Y_{1,i\neq k}}} \left.\frac{\mathrm{d}Y_{1,k}}{\mathrm{d}t}\right|_\mathrm{s} .\end{aligned} \tag{33}$$

where, again, each partial-derivative coefficient exists on the instantaneous shock Hugoniot and can be evaluated by differentiating the Rankine-Hugoniot relations.

The shock-derivative expansions, (32) and (33), can be substituted into (27). By grouping terms the desired result is obtained,

$$\begin{aligned}&\frac{1}{a_{\mathrm{f},1}}\frac{\mathrm{d}U_\mathrm{s}}{\mathrm{d}t}\frac{1}{\rho_1 a_{\mathrm{f},1}}\left(\frac{\partial P_2}{\partial w_1} + \rho_2 w_2\left(1-\frac{\partial w_2}{\partial w_1}\right)\right) \\ &\qquad = \frac{\rho_2 a_{\mathrm{f},2}^2}{\rho_1 a_{\mathrm{f},1}^2}\left(\dot{\sigma} - \eta\left.\frac{\partial u}{\partial x}\right|_2\right) - \frac{\Sigma}{\rho_1 a_{\mathrm{f},1}^2} ,\end{aligned} \tag{34}$$

where a partial normalization by $\rho_1 a_{\mathrm{f},1}^2$ was also introduced. Σ contains all terms associated with the upstream flow variation, which were extracted from the shock-derivative expansions, and can be concisely written as

$$\begin{aligned}\Sigma = \sum_{\alpha_1\in\mathcal{U}} &\left(\frac{\partial P_2}{\partial \alpha_1} - \rho_2 w_2 \frac{\partial w_2}{\partial \alpha_1}\right)\left.\frac{\mathrm{d}\alpha_1}{\mathrm{d}t}\right|_\mathrm{s}, \\ &\mathcal{U} = \{u_1, P_1, \rho_1, \mathbf{Y_1}\} .\end{aligned} \tag{35}$$

All partial derivatives are computed for constant shock speed, U_s, hence, for $\alpha_1 = u_1$, the corresponding term becomes

$$-\left(\frac{\partial P_2}{\partial w_1} - \rho_2 w_2 \frac{\partial w_2}{\partial w_1}\right)\left.\frac{\mathrm{d}u_1}{\mathrm{d}t}\right|_\mathrm{s} , \tag{36}$$

which recovers the form expressed in (33). Note that the subscripted terms have now been dropped from the partial derivatives to prevent cluttering the equations.

The first term on the left-hand side of (34), $\mathrm{d}U_\mathrm{s}/\mathrm{d}t$, is the shock wave acceleration. It is multiplied by a nondimensional coefficient we term here as H,

$$H = \frac{1}{\rho_1 a_{\mathrm{f},1}} \left(\frac{\partial P_2}{\partial w_1} + \rho_2 w_2 \left(1 - \frac{\partial w_2}{\partial w_1} \right) \right) . \quad (37)$$

Each term in this coefficient is given by the shock jump relations and the instantaneous upstream state.

On the right-hand side of (34) are source terms or forcing terms, which describe how the shock wave's acceleration originates from external flow gradients. If the forcing terms are zero, then the shock acceleration is zero, and the shock speed is constant.

4.1.1 Forcing Terms

The forcing terms can be grouped into those associated with the flow upstream of or ahead of the shock wave, F_1, and those associated with the flow downstream of or behind the shock wave, F_2. The contributions from the upstream and downstream flows can be separated because they occur on different sides of the shock-jump discontinuity. Using this nomenclature, the shock-change equation (34) can be written as

$$\frac{H}{a_{\mathrm{f},1}} \frac{\mathrm{d}U_\mathrm{s}}{\mathrm{d}t} = F_1 + F_2 \quad (38)$$

where

$$F_1 = -\frac{\Sigma}{\rho_1 a_{\mathrm{f},1}^2} \quad (39)$$

$$F_2 = \frac{\rho_2 a_{\mathrm{f},2}^2}{\rho_1 a_{\mathrm{f},1}^2} \left(\dot{\sigma} - \eta \left. \frac{\partial u}{\partial x} \right|_2 \right) \quad (40)$$

Chemical reactions require a finite time to occur, hence their total contribution to shock acceleration cannot be computed from the instantaneous post-shock thermicity. Although chemical reactions cannot be easily separated from other post-shock flows, the net effect on the shock wave is captured by the downstream forcing term, F_2.

The upstream forcing term (35) is valid for a generally nonuniform and unsteady upstream flow, described by the four linearly-independent quantities in the set $\mathcal{U}$. If only a single quantity is varying, then only that variable need be considered in (35). For example, if the shock is traveling through a nonuniform temperature field, then $\mathcal{U} = \{T_1\}$. Another important example is a nonsteady centered expansion, in which case the flow is described by a similarity solution, and the variation in upstream quantities can be expressed in terms of only the similarity variable, $\xi = x/t$. The reflected shock generated by detonation reflection is the relevant example of a shock wave that traverses a centered expansion of the opposite family, the TZ wave. In this case, Σ becomes

$$\Sigma = \left(\frac{\partial P_2}{\partial \xi_1} - \rho_2 w_2 \frac{\partial w_2}{\partial \xi_1} \right) \left. \frac{\mathrm{d}\xi}{\mathrm{d}t} \right|_\mathrm{s} , \quad (41)$$

where $\xi = X_\mathrm{s}/t$.

If the upstream flow is uniform, then $\Sigma = 0$ and the shock acceleration is given by

$$\frac{\mathrm{d}U_\mathrm{s}}{\mathrm{d}t} = \frac{\rho_2 a_{\mathrm{f},2}^2 \left(\dot{\sigma} - \eta \left. \frac{\partial u}{\partial x} \right|_2 \right)}{\frac{\partial P_2}{\partial w_1} + \rho_2 w_2 \left(1 - \frac{\partial w_2}{\partial w_1} \right)} . \quad (42)$$

4.1.2 Perfect Gas

The result (34) is valid for a general equation of state, however substantial simplification is obtained by considering a perfect gas. For a perfect gas, the shock-jump relations are well-known functions of only the ratio of specific heats, γ, and the shock Mach number. The shock Mach number is given by

$$M_\mathrm{s} = \frac{w_1}{a_1} = \frac{U_\mathrm{s} - u_1}{a_1} , \quad (43)$$

hence variation in both upstream velocity, u_1, and sound speed, a_1, must be considered when differentiating the shock jump equations.

For a perfect gas, (29) and (30) are

$$P_2 = P_1 \left(1 + \frac{2\gamma}{\gamma + 1} (M_\mathrm{s}^2 - 1) \right) \quad (44)$$

$$u_2 = u_1 + \frac{2a_1}{\gamma + 1} \frac{M_\mathrm{s}^2 - 1}{M_\mathrm{s}} \quad (45)$$

The set of relevant upstream variables then is

$$\mathcal{U} = \{u_1, P_1, a_1\} . \quad (46)$$

The shock acceleration coefficient (37) becomes

$$H = \frac{2}{\gamma + 1} \frac{3M_\mathrm{s}^2 + 1}{M_\mathrm{s}} , \quad (47)$$

and substituting it into (34) gives a shock-change equation for a perfect gas,

$$\frac{2}{\gamma+1}\frac{3M_s^2+1}{M_s}\frac{1}{a_1}\frac{\mathrm{d}U_s}{\mathrm{d}t} = F_1 + F_2 \tag{48}$$

where the forcing terms are

$$\begin{aligned} F_1 = &-\frac{(\gamma-5)M_s^2-2}{(\gamma+1)M_s}\frac{1}{a_1}\frac{\mathrm{d}u_1}{\mathrm{d}t}\bigg|_s \\ &-\left(1+\frac{2\gamma}{\gamma+1}(M_s^2-1)\right)\frac{1}{\rho_1 a_1^2}\frac{\mathrm{d}P_1}{\mathrm{d}t}\bigg|_s \\ &+\frac{4}{\gamma+1}(M_s^2+1)\frac{1}{a_1}\frac{\mathrm{d}a_1}{\mathrm{d}t}\bigg|_s \\ F_2 = &\frac{P_2}{P_1}\left(\dot{\sigma}-\eta\frac{\partial u}{\partial x}\bigg|_2\right) . \end{aligned} \tag{49}$$

For the case of a shock traveling through a centered expansion, such as the TZ wave, then the upstream forcing term is

$$F_1 = \frac{2}{\gamma+1}\left(\frac{2(M_s+1)^3}{(\gamma+1)M_s} - M_s - 3\right)\frac{M_s+1}{t} \tag{50}$$

where this result is valid for a right-running shock wave traversing a left-running expansion wave.

4.2 Application to Simulation Results

The simulation results from sections 3.2 and 3.3 can now be analyzed using the derived shock-change equation for a one-gamma perfect gas (48). In particular, at each time step the forcing terms can be computed using (49), and their magnitude and sign describe how the observed shock acceleration results from the upstream and downstream flows.

4.2.1 Supported Detonation

The net forcing terms are plotted in Fig. 17. Fig. 17(a) shows that the magnitude of both forcing terms rapidly decreases as the shock propagates away from the wall. Initially, the downstream forcing term, F_2, is negative, and it remains negative until much later at $t \approx 91$. The upstream forcing term, F_1, is positive for all simulation time, monotonically approaching zero. The absolute magnitude of the forcing terms, plotted in 17(b), intersect at $t \approx 4$, which means that the net forcing term is zero and the shock acceleration goes to zero. This is illustrated in Fig. 7 by the shock velocity maximum.

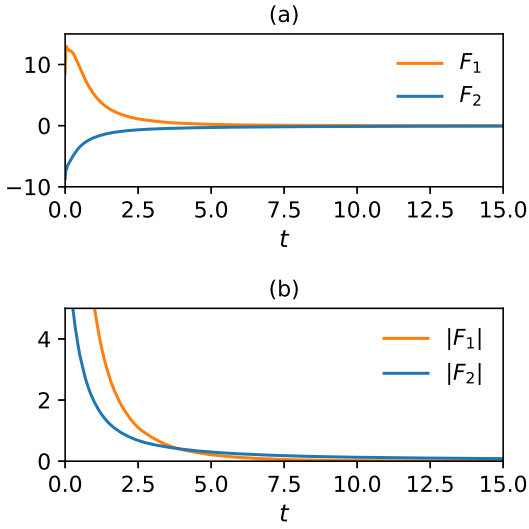

Fig. 17 Upstream and downstream forcing terms plotted over time for a shock reflected by a supported detonation. (a) shows the signed value of the terms, and (b) shows the absolute magnitude

These results clarify the factors that cause the shock acceleration from Fig. 7. The reflected shock rapidly accelerates from the vN reflection speed to substantially overshoot the CJ reflection limit. The large initial acceleration to an elevated near-wall speed is caused by the shock's propagation through the large gradients in the incident detonation's reaction zone. The large gradients cause the large, positive upstream forcing term illustrated in Fig. 17. The acceleration and elevated shock speed are not caused by post-shock chemical reactions, since the net downstream forcing term is negative in early time, which means that the positive contribution from chemical reaction is nonetheless smaller than the negative contribution from the post-shock velocity gradient.

Upon rapidly accelerating, the reflected shock reaches a peak velocity and begins to decay at a slower rate. After propagating through the incident detonation's reaction zone structure, the upstream forcing rapidly approaches zero, while the negative downstream forcing persists from the post-shock velocity gradient. The result is that the forcing terms balance and a maximum shock speed is reached. Subsequently, the forcing terms are smaller and decreasing in magnitude, so the shock decay toward the asymptotic value elapses over a longer time than the initial shock acceleration.

4.2.2 Unsupported Detonation

The upstream and downstream forcing terms are plotted for early time in Fig. 18(a) and (b), respectively. The magnitude of both upstream and downstream terms rapidly decreases as time elapses. The upstream forcing terms are positive for all time, and the downstream forcing terms are negative for all time. The downstream forcing terms are nearly indistinguishable for the different domain lengths, however the upstream forcing terms level off to greater values for the smaller domain lengths.

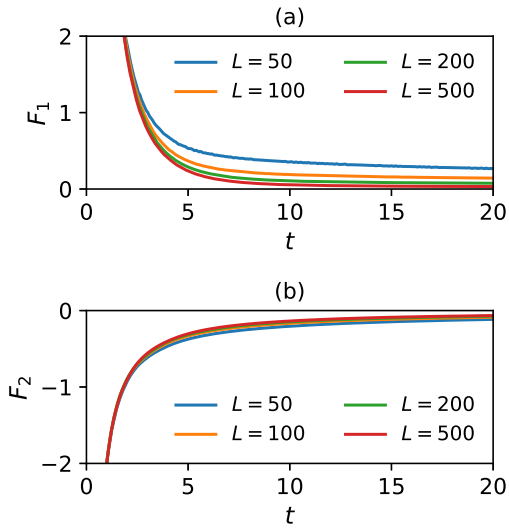

Fig. 18 Shock acceleration forcing terms for (a) upstream and (b) downstream flows from unsupported detonation reflection

The absolute magnitude of the forcing terms are plotted against time for the four domain lengths in Fig. 19. The plot limits are chosen so that the important variations in forcing terms are visible as the shock propagates through the incident detonation and into the TZ wave. In all cases, when the reflected shock reaches the end of the TZ wave, the upstream state becomes uniform and so the upstream forcing term is instantaneously zero. This is later in time and not shown in Fig. 19. Fig. 19(a) and (b) show that $|F_1|$ is greater than $|F_2|$ for all time until the shock reaches the end of the TZ wave. In Fig. 19(b) the curves for $|F_1|$ and $|F_2|$ come closer to each other, approaching a point of near tangency. Fig. 19(c) and (d) show that the upstream forcing term intersects the downstream forcing term, $|F_2|$, twice, resulting in two points where the forcing terms balance, and the shock acceleration goes to zero. These two points correspond with the local maxima and minima in Fig. 13.

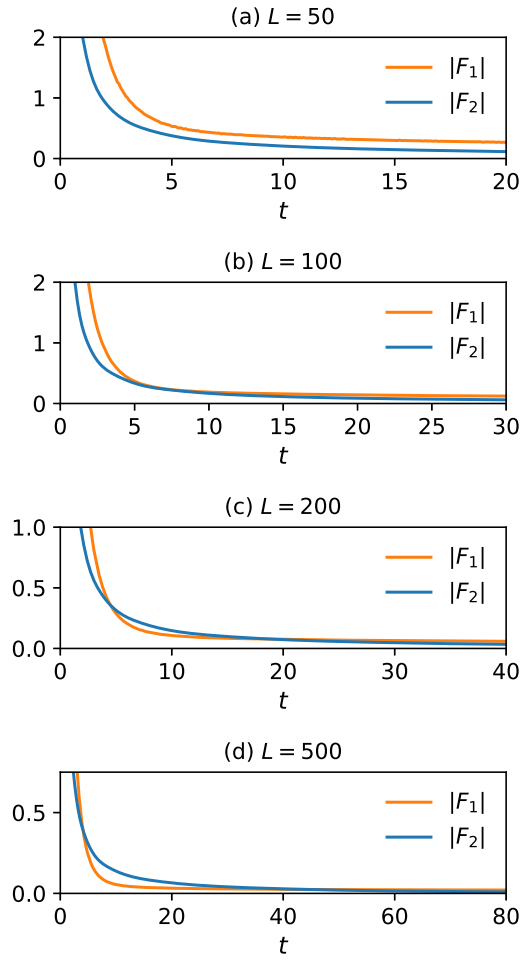

Fig. 19 Magnitude of upstream and downstream forcing terms computed from unsupported detonation reflection simulation for four domain lengths

As the size of the domain increases relative to the detonation thickness, there is a distinct transition in reflected shock evolution as illustrated by the shock velocities in Fig. 13 and the forcing terms in Fig. 19. For short domain lengths, $L = 50$ and $L = 100$, the shock speed monotonically increases until reaching the end of the TZ wave, whereas minima and maxima shock velocities form near the end wall for longer domain lengths, $L = 200$ and $L = 500$. Fig. 19 shows that these shock acceleration behaviors result from a

transition in how upstream and downstream forcing terms are balanced.

The supported detonation results illustrated that the upstream forcing term, although initially large, rapidly decays as the shock propagates through the incident detonation into a region of uniformity. For the unsupported detonation, the shock subsequently propagates into the TZ wave, and hence the shock acceleration is determined by the relative magnitude between the positive forcing by the TZ wave and the negative forcing from the nonsteady waves that persist from propagation through the reaction zone. This can be illustrated by evaluating the forcing terms when the shock passes through the incident detonation's sonic point, since the sonic point represents a transition between flows dominated by the detonation reaction zone structure and the TZ wave, respectively. The magnitude of the forcing terms at the sonic point are plotted in Fig. 20. For $L = 50$ and 100, the upstream forcing is greater, however for $L = 200$ and 500 the downstream forcing is greater. This illustrates the balance between forcing terms that yields the shock acceleration and forcing term trends observed in Fig. 13 and 19. The length that corresponds to the intersection in Fig. 20 is the point where the forcing terms balance exactly. Since the shock acceleration is positive before and after this point, the equivalent plot of forcing term magnitudes, as shown in Fig. 19, would show a tangency between curves.

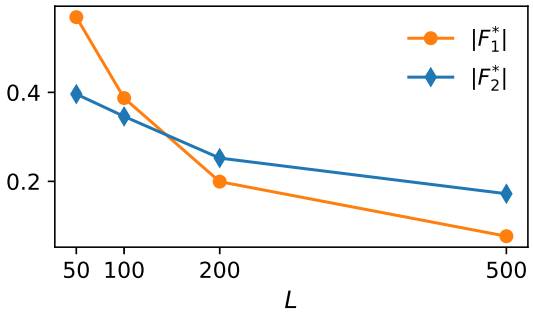

Fig. 20 Magnitude of upstream and downstream forcing terms evaluated when the reflected shock arrives at the incident detonation's sonic point for the four simulated domain lengths

5 Discussion

The numerical simulation results demonstrate the importance of a finite detonation thickness on the dynamics of the reflected shock wave. The subsequent analysis with the derived shock-change equation identified that the primary cause of the reflected shock acceleration is the highly-nonuniform flow through which the shock propagates. The shock reflected by a finite-thickness detonation responds instantaneously to the large upstream gradients and rapidly accelerates through the detonation thickness to a large shock speed, overshooting the limiting value predicted by reflection of a zero-thickness detonation. The reflected shock's propagation through upstream nonuniformity reflects nonsteady waves, and their net influence on the shock manifests in the shock-change equation through the post-shock velocity gradient. Nonsteady waves persist after the reflected shock has propagated through a region of nonuniformity and act to decrease the shock speed until the post-shock flow velocity is uniformly zero, matching the boundary condition. As a consequence, the large reflected shock velocities persist for significant time after the shock has already propagated through the incident detonation, so the effects of finite detonation thickness influence the reflected shock for distances that are large relative to the detonation thickness. A measure for this distance is given by the time when the speed of the shock reflected by the supported detonation first intersects the limiting value. This occurs in the simulation at time $t = 77.6$ and distance $x = 37.5$.

The results obtained here for a one-gamma, one-step detonation model are qualitatively consistent with experimental observations of reflected shock behavior from real, multidimensional detonations. Damazo and Shepherd [13] performed highly-resolved measurements of normal detonation reflection in a 7.67-meter-long detonation tube. They observed that the near-wall reflected shocks propagated with a shock velocity substantially greater than expected from ideal modeling that neglects the detonation thickness. Damazo and Shepherd proposed that the effect was due to explosion of the twice-shocked reactants in the incident detonation's induction zone behind the reflected shock. Coupling between post-shock thermodynamics and reaction rate may result in a substantially overdriven reflected detonation that subsequently drives a shock wave at a speed much faster than predicted by equilibrium calculations alone. The use of a one-step reaction mechanism with reduced activation energy precludes evaluation of this effect, since the thermodynamics and reaction rate were intentionally decoupled to stabilize the unsupported detonation. Despite this,

the simulation results capture similar shock dynamics because they are caused principally by the shock's propagation through the large flow nonuniformities in the incident detonation. Positive contributions to the reflected shock acceleration from post-shock chemical reactions, although present, were entirely negated by the large velocity-gradient behind the shock. This was shown by the signed upstream and downstream forcing terms in the shock-change equation. The essential influence of the upstream nonuniformity on reflected shock acceleration is expected to be a general aspect of the problem of normal detonation reflection. However, the relative importance of chemical reactions cannot be generalized from the present results due to the inherent modeling limitations.

The conclusion that upstream nonuniformity causes significant shock acceleration and provides an explanation for the elevated reflected shock speeds observed in experiment can also be arrived at using a simple "square-wave" detonation model. This approach was used by Damazo and Shepherd [13] to evaluate the contribution from chemical reaction, however similar results are obtained with calculations using a frozen thermodynamic state. The problem is to predict the shock transmitted when the vN reflected shock impacts the square-wave boundary between the frozen and equilibrium states, i.e., when the vN reflected shock impacts the incident CJ state. The solution for the one-gamma model used here is $U_{\mathrm{s}} = 0.83$. From section 2, the vN and CJ reflected shock speeds are 0.2 and 0.41, respectively. The transmitted shock speed is substantially greater than the speed of the CJ reflected shock, illustrating that the result is due to the jump in upstream flow quantities.

A ramification of the finite detonation thickness is that there is a period of very large increased pressure at the reflecting end wall. Detonation reflection calculations are often used to evaluate peak pressures in detonation tubes, where it is common to consider the CJ reflection value, approximately 2.5 times the CJ pressure [2]. The excess impulse per unit area from the finite detonation thickness exerted on the end wall was found to be 26.8 for the supported detonation reflection. This was exerted over approximately $\Delta t = 16.4$, giving a mean excess pressure over this period of approximately 1.6 times the CJ pressure. The excess impulse was found to be approximately the same for the unsupported detonations. If a real detonation has thickness on the order of a millimeter with CJ speed of approximately $2\ \mathrm{mm}/\mu\mathrm{s}$, then this period of excess pressure is on the order of microseconds. The pressure decays very rapidly, so for thin detonations the transient pressure is likely often lost during measurement with transducers because of large vibrational noise that results from detonation impact and limited-bandwidth instrumentation. The duration of excess pressure scales with detonation thickness, so for suitably thick detonations the pressure pulse may be observable.

6 Conclusion

Normal detonation reflection is an under-examined aspect of detonation and shock physics. As shown in this paper, even for a rather simple detonation model, significant complexity results.

The problem was formulated in one dimension in terms of a one-gamma, one-step detonation model with reduced activation energy and studied using numerical simulation of both a supported and unsupported detonation. Results showed novel dynamics as the shock propagated through the various regions of nonuniformity in a detonation. A shock-change equation, valid for a nonuniform upstream flow, was derived in terms of shock acceleration caused by forcing terms, which describe the separate influences of the upstream and downstream flows. These methods were used to analyze simulation results to show the exact underlying factors causing the observed shock dynamics.

Rapid shock acceleration to an elevated initial velocity was found to be caused by shock propagation through the large nonuniformities in the detonation reaction zone. The elevated velocity persists for substantial time, such that the detonation thickness relative to the pipe length must be much smaller than might be expected in order to use the ideal detonation assumption used by prior modelers. For short pipes, the positive forcing by the TZ wave was large enough that the reflected shock velocity increased monotonically until reaching the end of the TZ wave.

A highly simplified detonation model was used to perform this analysis, and so there are several areas where the modeling could be improved to better understand real detonation reflection. Larger activation energies could be implemented with the present approach and would allow greater coupling between the post-shock thermodynamics and reaction rate. While still one-dimensional, more detailed reaction mechanisms could be employed. Multidimensional effects might be investigated with simulations

and similarly analyzed using shock-change methods, generalized to include shock curvature.

Acknowledgments. This work was sponsored by the Office of Naval Research (ONR), under grant number N00014-22-1-2141. The views and conclusions contained herein are those of the authors only and should not be interpreted as representing those of ONR, the U.S. Navy or the U.S. Government.

References

[1] Stanyukovich, K.I.: Unsteady Motion of Continuous Media. Pergamon Press, London (1960). https://doi.org/10.1016/C2013-0-08194-7

[2] Shepherd, J.E., Teodorcyzk, A., Knystautas, R., Lee, J.H.: Shock Waves Produced by Reflected Detonations. Progress in Astronautics and Aeronautics **134**, 244–264 (1991)

[3] Karnesky, J., Damazo, J., Chow-Yee, K., Rusinek, A., Shepherd, J.E.: Plastic deformation due to reflected detonation. Int. J. Solids Struct. **50**(1), 97–110 (2013). https://doi.org/10.1016/j.ijsolstr.2012.09.003

[4] Strachan, J.D., Huni, J.P., Ahlborn, B.: Shock propagation into inhomogeneous media. J. Fluid Mech. **43**(3), 487–495 (1970). https://doi.org/10.1017/S0022112070002537

[5] Chisnell, R.F.: The normal motion of a shock wave through a non-uniform one-dimensional medium. Proc. Math. Phys. Sci. **232**(1190), 350–370 (1955). https://doi.org/10.1098/rspa.1955.0223

[6] Schoeffler, D.T., Shepherd, J.E.: Modeling Detonation Reflection with Nonsteady Shock Change Equation. 28th International Colloquium on Dynamics of Explosions and Reactive Systems, vol. Paper 73. Napoli, Italy (2022)

[7] Liang, Z., Karnesky, J., Shepherd, J.E.: Structural response to reflected detonations and deflagration-to-detonation transition in H2-N2O mixtures. Technical Report EDL FM2006.003, GALCIT (2006)

[8] Liang, Z., Karnesky, J., Shepherd, J.E., Deiterding, R.: Detonations in C2H4-O2. experimental measurements and validation of numerical simulation for incident and reflected waves. Technical Report EDL FM2006.009, GALCIT (2008)

[9] Karnesky, J., Damazo, J., Shepherd, J.E., Rusinek, A.: Plastic Response of Thin-Walled Tubes to Detonation. Pressure Vessels and Piping Conference, vol. ASME 2010 Pressure Vessels and Piping Conference: Volume 4, pp. 263–277 (2010). https://doi.org/10.1115/PVP2010-25749

[10] Damazo, J., Ziegler, J., Karnesky, J., Shepherd, J.E.: Shock Wave–Boundary Layer Interaction from Reflecting Detonations. 28th International Symposium on Shock Waves, pp. 751–756 (2012). https://doi.org/10.1007/978-3-642-25685-1_114

[11] Damazo, J., Shepherd, J.E.: Reflected Detonation Waves: Comparing Theory to Pressure and Heat Flux Measurements. 29th International Symposium on Shock Waves, vol. 1, pp. 325–327 (2015). https://doi.org/10.1007/978-3-319-16835-7_50

[12] Damazo, J.S.: Planar reflection of gaseous detonation. PhD thesis, California Institute of Technology (2013). https://doi.org/10.7907/4QW7-TK55

[13] Damazo, J., Shepherd, J.E.: Observations on the normal reflection of gaseous detonations. Shock Waves **27**, 795–810 (2017). https://doi.org/10.1007/s00193-017-0736-6

[14] Fickett, W., Davis, W.C.: Detonation. University of California Press, Berkeley (1979)

[15] Lee, J.H.S.: The Detonation Phenomenon. Cambridge University Press, New York (2008). https://doi.org/10.1017/CBO9780511754708

[16] Radulescu, M.I., Sharpe, G.J., Law, C.K., Lee, J.H.S.: The hydrodynamic structure of unstable cellular detonations. J. Fluid Mech. **580**, 31–81 (2007). https://doi.org/10.1017/S0022112007005046

[17] Short, M., Quirk, J.J.: On the nonlinear stability and detonability limit of a detonation wave for a model three-step chain-branching reaction. J.

Fluid Mech. **339**, 89–119 (1997). https://doi.org/10.1017/S002211209700503X

[18] Austin, J.M.: The Role of Instability in Gaseous Detonation. PhD thesis, California Institute of Technology (2003). https://doi.org/10.7907/X7YH-T687

[19] Radulescu, M.I., Sharpe, G.J., Lee, J.H.S., Kiyanda, C.B., Higgins, A.J., Hanson, R.K.: The ignition mechanism in irregular structure gaseous detonations. Proceedings of the Combustion Institute **30**(2), 1859–1867 (2005). https://doi.org/10.1016/j.proci.2004.08.047

[20] Lee, H.I., Stewart, D.S.: Calculation of linear detonation instability: one-dimensional instability of plane detonation. J. Fluid Mech. **216**, 103–132 (1990). https://doi.org/10.1017/S0022112090000362

[21] Taylor, G.I.: The dynamics of the combustion products behind plane and spherical detonation fronts in explosives. Proc. Math. Phys. Sci. **200**(1061), 235–247 (1950). https://doi.org/10.1098/rspa.1950.0014

[22] OpenFOAM. The OpenFOAM Foundation Ltd. https://openfoam.org/

[23] blastFoam: A Solver for Compressible Multi-Fluid Flow with Application to High-Explosive Detonation. Synthetik Applied Technologies, LLC. (2020). https://github.com/synthetik-technologies/blastfoam

[24] Thompson, P.A.: Compressible Fluid Dynamics. McGraw-Hill, New York (1972)

[25] Goodwin, D.G., Moffat, H.K., Speth, R.L.: Cantera: An Object-Oriented Software Toolkit for Chemical Kinetics, Thermodynamics, and Transport Processes. https://www.cantera.org. Version 2.5.1 (2021). https://doi.org/10.5281/zenodo.4527812

[26] Kao, S.T.: Detonation Stability with Reversible Kinetics. PhD thesis, California Institute of Technology (2008). https://doi.org/10.7907/H8JN-VS03

[27] McBride, B.J., Gordon, S., Reno, M.A.: Coefficients for Calculating Thermodynamic and Transport Properties of Individual Species. Technical Memorandum TM-4513, NASA (1993)

[28] Kao, S.T., Ziegler, J.L., Bitter, N.P., Schmidt, B.E., Lawson, J., Shepherd, J.E.: SDToolbox: Numerical Tools for Shock and Detonation Wave Modeling. GALCIT Report FM2018.001, California Institute of Technology, Pasadena, CA (March 2020). http://shepherd.caltech.edu/EDL/PublicResources/sdt/

[29] Boyack, K.W., Tieszen, S.R., Stamps, D.W.: Internal pressure loads due to gaseous detonations. Proc. Math. Phys. Sci. **443**(1918), 343–366 (1993). https://doi.org/10.1098/rspa.1993.0150

[30] Sharma, V.D., Radha, C.: On one-dimensional planar and nonplanar shock waves in a relaxing gas. Phys. Fluids **6**(6), 2177–2190 (1994). https://doi.org/10.1063/1.868220

[31] Sharma, V.D., Venkatraman, R.: Evolution of weak shocks in one dimensional planar and non-planar gasdynamic flows. Int. J. Non-Linear Mech. **47**(8), 918–926 (2012). https://doi.org/10.1016/j.ijnonlinmec.2012.06.001

[32] Chen, P.J., Gurtin, M.E.: Growth and Decay of One-Dimensional Shock Waves in Fluids with Internal State Variables. Phys. Fluids **14**(6), 1091–1094 (1971). https://doi.org/10.1063/1.1693568

[33] Bowen, R.M., Chen, P.J.: Shock waves in a mixture of linear elastic materials. Rendiconti del Circolo Mat. di Palermo **21**(3), 267–283 (1972). https://doi.org/10.1007/BF02843791

[34] Nunziato, J.W.: One-dimensional shock waves in a chemically reacting mixture of elastic materials. J. Chem. Phys. **58**(3), 961–965 (1973). https://doi.org/10.1063/1.1679352

[35] Kennedy, J.E., Nunziato, J.W.: Shock-wave evolution in a chemically reacting solid. J. Mech. Phys. Solids **24**(2-3), 107–124 (1976). https://doi.org/10.1016/0022-5096(76)90021-1

[36] Radulescu, M.I.: On the shock change equations.

Phys. Fluids **32**(5), 056106 (2020). https://doi.org/10.1063/1.5140216

[37] Radulescu, M.I., Mével, R., Xiao, Q., Gallier, S.: On the self-similarity of diffracting gaseous detonations and the critical channel width problem. Phys. Fluids **33**(6), 066106 (2021). https://doi.org/10.1063/5.0054219

[38] Walsh, E.K.: Development of Shock Waves in Atmospheres with Density and Temperature Variation. Phys. Fluids **12**(4), 757–763 (1969). https://doi.org/10.1063/1.1692552

[39] Nunziato, J.W., Walsh, E.K.: Propagation and Growth of Shock Waves in Inhomogeneous Fluids. Phys. Fluids **15**(8), 1397–1402 (1972). https://doi.org/10.1063/1.1694099

[40] Nunziato, J.W., Walsh, E.K.: Shock-wave propagation in inhomogeneous atmospheres. Phys. Fluids **16**(4), 482–484 (1973). https://doi.org/10.1063/1.1694370

[41] Whitham, G.B.: On the propagation of shock waves through regions of non-uniform area or flow. J. Fluid Mech. **4**(4), 337–360 (1958). https://doi.org/10.1017/S0022112058000495

[42] Collins, R., Chen, H.T.: Motion of a shock wave through a nonuniform fluid. Proceedings of the Second International Conference on Numerical Methods in Fluid Dynamics, vol. 8, pp. 264–269 (1971). https://doi.org/10.1007/3-540-05407-3_39

[43] Catherasoo, C.J.: Shock Dynamics in Non-Uniform Media. PhD thesis, California Institute of Technology (1982). https://doi.org/10.7907/7knb-5s50

[44] Catherasoo, C.J., Sturtevant, B.: Shock dynamics in non-uniform media. J. Fluid Mech. **127**, 539–561 (1983). https://doi.org/10.1017/S0022112083002876

[45] Best, J.P.: A generalisation of the theory of geometrical shock dynamics. Shock Waves **1**(4), 251–273 (1991). https://doi.org/10.1007/BF01418882

[46] Vincenti, V.G., Kruger, C.H.: Introduction to Physical Gas Dynamics. Wiley, New York (1965)